Synthetic, physical and computational chemistry of propeller-shaped polycyclic aromatic hydrocarbons

Ham, A. van der

Citation

Ham, A. van der. (2022, February 24). *Synthetic, physical and computational chemistry of propeller-shaped polycyclic aromatic hydrocarbons*. Retrieved from https://hdl.handle.net/1887/3276776

Chapter 5

Freestanding Non-covalent Thin Films of the Propeller-shaped Polycyclic Aromatic Hydrocarbon Decacyclene

Abstract

Whereas the previous Chapters were concerned with the synthesis and conformational behavior of propellerenes, this chapter will focus on their supramolecular behavior. Although van der Waals forces are often responsible for the poor solubility of aromatic molecules, it will be shown here that these interactions can in fact be exploited to form mechanically stable, nanometer thin films, capable of being freestanding over micrometer distances. Using a combination of computational chemistry and microscopic imaging techniques, these thin films will be studied on the molecular and macroscale. The mechanical strength of these films will be probed and quantified using state-of-the-art AFM nano-indentation experiments. Self-assembled thin films, which are mechanically stable upon formation, without the requirement for further crosslinking, constitute the ultimate goal of reticular chemistry and the results reported here constitute a first step towards this goal.

Parts of this Chapter are published as:
van der Ham A., Liu X., Calvani D., Melcrova A., Kozdra M., Buda F., Overkleeft H. S., Roos W., Filippov D.V., Schneider G.F. **Manuscript accepted for publication in Nat. Comm.**

Nanometer thin, porous membranes hold promise for a wide range of applications, ranging from hydrogen fuel cells and desalination, to biomedical applications and nanoelectronics.[1-7] The particular interest in nanometer thin membranes stems from the fact that such membranes constitute the best trade-off between permeability and selectivity.[8,9] This is in part due to a significantly diminished hydrodynamic resistance towards water molecules, and by being less prone to fouling and clogging of pores.[10] When designing novel membranes, control over the functionality of the membrane, in terms of chemical composition, thickness, pore size and pore charge is therefore crucial. One particularly successful approach to make nanometer thin membranes is through molecular self-assembly (MSA),[11-13] which allows membrane properties to be tuned by incorporation of specific functional groups into the molecular building blocks used to make the membrane. However, a major hurdle in the development of such bottom-up membranes is the requirement to crosslink the individual building blocks, to achieve mechanical stability. This is typically achieved either *via* the incorporation of reactive functional groups into the monomeric building blocks, by thermal annealing,[14,15] photon[16] or electron irradiation.[17] These techniques often lead to loss of chemical definition, resulting in poor sample-to-sample reproducibility. Bottom-up membrane formation, without the need for annealing but with good mechanical stability thus constitutes the ultimate goal. Within the field of reticular chemistry, several types of 2D non-covalent organic frameworks (non-COFs), like supramolecular organic frameworks (SOHs) and hydrogen-bonded organic frameworks (HOFs) are at the forefront of development in this direction.[18-21] Although a supramolecular framework based purely on π- π stacking interactions was recently reported, this existed in the form of a crystalline solid.[22] Entirely 2D thin films based solely on non-covalent interactions between aromatic small molecules, like the one reported here, are not known in the literature to date.

Langmuir-Blodgett (LB) thin films composed of the small propellerene, decacyclene, have previously being developed for use in light-emitting devices.[23,24] The stacking behavior of this molecule and the mechanical properties of these thin films were, however, unexplored. The present study therefore starts with simulation assemblies of decacyclene molecules on a water surface using Molecular Dynamics (MD) simulations, in conjunction with DFT computations, to get a molecular picture of the packing of decacyclene at the air-water interface. Thin films are then produced, and a range of high-resolution microscopic techniques (AFM, SEM and TEM) used to get a microscopic image of the thin films. The van der Waals forces, which hold the molecules in these thin films together, were found to be strong enough to allow them to be free-standing over micrometer distances. State-of-the-art AFM nanoindentation then quantify the mechanical strength of these unique thin films.

Decacyclene thin films constitute the first PAH-based, non-covalent thin films, with a mechanical strength on par with that of known non-covalent membranes. These results therefore serve as an important step towards the fabrication of mechanically stable membranes, not requiring annealing.

Decacyclene[25] thin films were prepared in a KSV minithrough, using Millipore® ultrapure water as subphase. Thin films were subjected to several compression-decompression cycles and the surface pressure monitored throughout (Fig. 5.1A and B). A strong hysteresis was observed, showing smaller mean molecular areas with each cycle, going from an initial onset of 40 Å^2 / molecule to only 22 Å^2 / molecule.[26] This indicates that the decacyclene monolayer is unstable at the air-water interface, and molecular rearrangements take place during the compression process. These molecular rearrangements entail the adaptation of a thermodynamically more favorable orientation of the molecules in the monolayer, which is known to be the direct result of factors such as intermolecular interactions, phase transitions and lateral diffusion.[27]

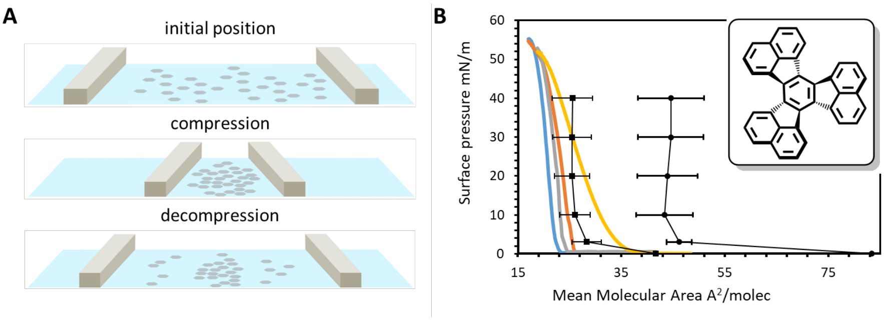

Figure 5.1 Langmuir-Blodgett experiments and thin film formation of decacyclene. (A) Schematic representation of the compression-decompression of decacyclene molecules at the air-water interface in a Langmuir-Blodgett through. (B) Representative experimental Langmuir-Blodgett isotherms for two consecutive compression/decompression cycles on a single sample, showing surface pressure as a function of mean molecular area. Black lines are isotherms computed using MD simulations, for systems containing 30 (●) and 60 (■) molecules, respectively. Reported values are averaged over 3 separate MD simulations with error bars indicating standard deviations. Insert shows the molecular structure of decacyclene.

Molecular Dynamics Simulations. To study the molecular processes taking place at the air-water interface during the compression, Molecular Dynamics (MD) simulations were performed. The model system used consisted of a box of water molecules, with a total of 30 or 60 decacyclene molecules on each side (Fig. 5.2A and 5.2B). Input geometries for decacyclene were obtained from DFT computations at PBE/6-31G(d,p). Optimized geometries with a D_3 symmetry were computed to be thermodynamically preferred over those with a C_2 symmetry (ΔG_{gas} = –0.3 kcal mol^{-1}; Fig. S5.2), in line with crystallographic data.[28] After pre-equilibration of the system at 300 K, the average intermolecular distance between decacyclene molecules was found to be ~3.6 Å (Fig. 5.2C), which is in good agreement with that computed with DFT for a decacyclene dimer (3.68 Å), (Fig. 5.1C)[29] and crystallographically (3.9 Å).[30]

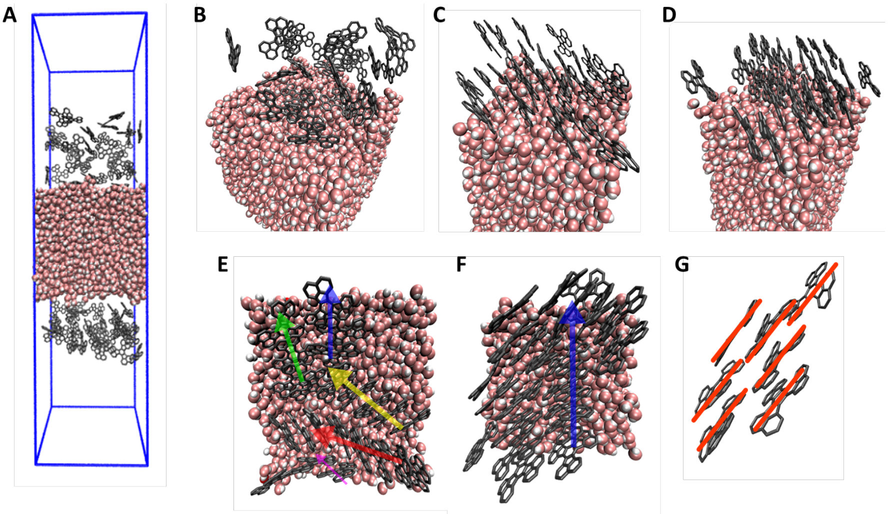

Figure 5.2 Molecular Dynamics (MD) simulation on decacyclene thin films. (A), MD simulation box (5.0 x 5.0 x 20.0 nm^3) containing water molecules represented by a space filling model, and the random, pre-equilibration position of decacyclene molecules (30) on both sides thereof represented by a liquorice model in grey. Protons explicitly drawn on water but omitted from decacyclene. (B) Top view of A. (C) Same system as B, after equilibration at 300 K. (D) Same system as C, after compression to a surface pressure of 30 mN m^{-1}. (E) Top view of D after equilibration at 300 K. Differently colored arrows added to highlight different stacking domains. (F) Same system as in E after compression to a surface pressure of 30 mN m^{-1}. (G) Highlight of molecules found in F showing the onset of roof-tiling.

In all cases, a parallel stacking mode was found most favorable. In the MD simulations, the stacked molecules were found to align themselves perpendicularly to the water surface, forming distinct domains with different relative orientations (Fig. 5.2D–F). Intuitively, such an arrangement decreases the total surface area of the hydrophobic, decacyclene molecules with the water surface. These findings thus served as an initial validation that the MD model is able to accurately describe the intermolecular interactions in this system. Note that decacyclene was previously found experimentally to have an intrinsic preference to absorb parallel to the surface of copper(100) foil.[31,32]

After pre-equilibration of the system, the surface area of the simulation box was reduced in the x-y plane, corresponding to an increase in surface pressure in the Langmuir-Blodgett compression technique. Plotting of the surface pressure as a function of the Mean Molecular Area (MMA) thus yields an isotherm, which can be compared to those obtained experimentally (Fig. 5.1B). Systems containing 30 and 60 decacyclene molecules were modelled. In former case, a monolayer of molecules was found with an average MMA of approximately 44 Å^2/molecule; in the latter case, a bimolecular layer is obtained, with an MMA of roughly 26 Å^2/molecule. The computed isotherm for the bimolecular layer system was found to be in reasonable agreement with experimental data. In both cases, upon compression, molecules in their distinct domains were found to intercalate with neighboring domains to adopt a slipped stacking mode, a process called "roof-tiling" (Fig. 5.2G).[33] When using a racemic mixture of D_3 conformers, *i.e.* containing equal numbers of (+) and (–) rotating molecules, distinct domains are still formed, containing a random mixture of isomers. Such systems give isotherms identical to optically pure systems (SI Fig. S5.5). Apart from domain reformations, a change in the orientation of the molecules relative to the water surface is also observed upon compression. Quantification of the tilt angle (*i.e.* the angle of the plane of a decacylene molecule to the surface of water), revealed that, upon compression, the preferred tilt angle shifts from 50 to almost 90 degrees, driven by a desire to minimize the contact area with the water surface (Fig. 5.3).

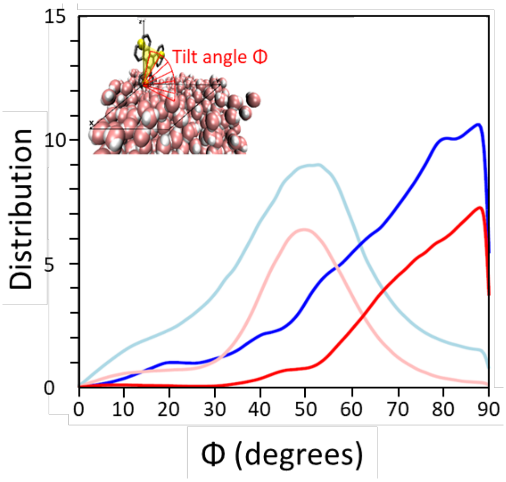

Figure 5.3 Distribution of the tilt angle (Φ) per decacyclene molecule as derived from the MD simulations. The definition of the tilt angle (Φ) as the arc between the plane of a decacyclene molecule (yellow) and the x-y plane of the water surface, is illustrated in the top left. Shown are the distributions of the tilt angles for systems consisting of 60 (blue) and 30 (red) decacyclene molecules, before (light) and after (dark) compression to a surface pressure of 30 mN m^{-1}. Distribution curves were obtained *via* Gaussian broadening with default standard deviation and normalized per amount of decacyclene molecules, using a Kernel Density Estimation to produce this plot with N_{bins} = 1897.

To characterize the thin films on a microscopic scale, samples were transferred unto a Si/SiO_2 wafer by horizontal lifting at constant pressure (25 mN m^{-1}) and imaged using atomic force microscopy (AFM) (Fig. 5.4A). This showed a uniform coverage of the substrate by the thin film, with a thickness of 2.49 ± 1.25 nm (Fig. 5.4B), corresponding roughly to a bimolecular layer. This average thickness corresponds nicely with the bimolecular layer obtained from the MD simulations (*vide supra*). No crystallinity of the thin film was found with transmission electron microscopy (TEM; data not shown). To test the mechanical stability of the thin film, samples were transferred onto a copper TEM grid, covered with holey Quantifoil®.[34] Using scanning electron microscopy (SEM), thin films were found capable of being free-standing over 0.6 and 1.0 µm diameter apertures with only minimal defects (Fig. 5.4C). Transfer onto a 2 µm holey grid showed thin films could be free-standing even over these larger distances (Fig. 5.4D), yet with less reproducibility.

As the thin films are able to be free-standing, without having required any form of annealing, it became interesting to quantify their mechanical strength. This was done using AFM nanoindentation experiments,[35,36] using samples transferred onto a golden TEM grid covered with holey UltrAufoil®.[37] Initial images of the free-standing thin films showed a small height increase depicted as a lighter color around the perimeter of the aperture (Fig. 5.4D, Fig. S5.6, Fig. S5.7, ø = 1 μm). The thin films themselves were found to recede slightly into the apertures as a result of the van der Waals attraction between the thin film and the TEM substrate (Fig. S5.7B). The same effect was previously observed for graphene,[36,38] as well as for nanoparticle-based free-standing membranes.[39]

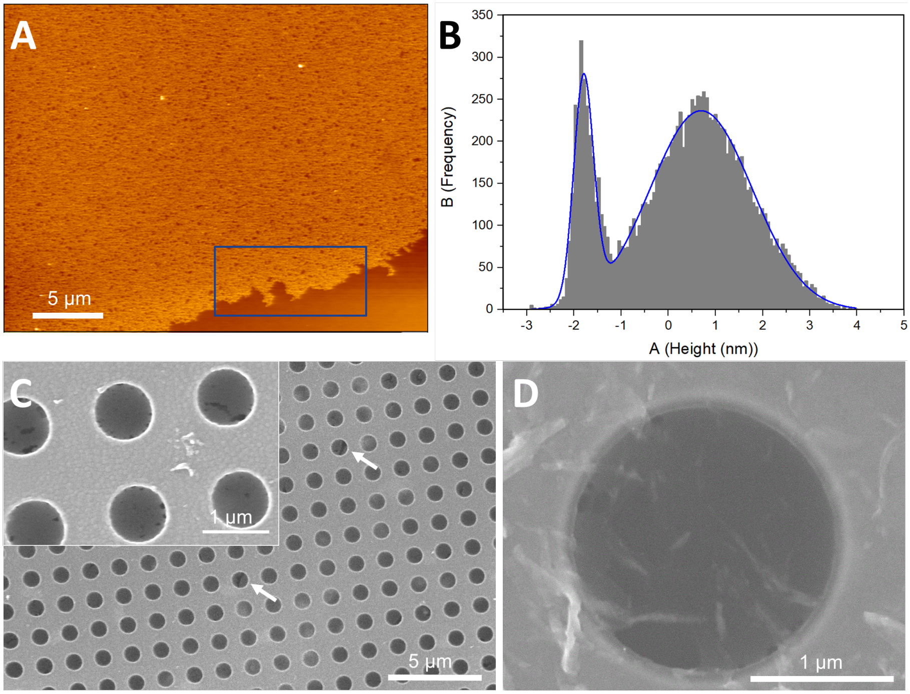

Figure 5.4 (A) AFM image of a decacyclene film transfered unto a Si/SiO$_2$ wafer. (B) Height profile of the area marked in blue in A, showing a film thickness of 2.49 ± 0.71 nm. (C) SEM image of a decacyclene film free-standing over 0.6 μm diameter apertures. Ruptured films are indicated by arrows. Insert shows a zoom on the same grid, illustrating minor film defects as dark regions. (D) SEM image of a near-defect free decacyclene film free-standing over a 2 μm aperture.

The freestanding thin films were indented in the center of the circular apertures with an AFM tip (nominal radius 2 nm) until failure of the decacyclene film occurred (Fig. 5.5A-B, Fig. S5.6). For every indentation, the depth of the indentation by the AFM tip was plotted as a function of the applied force (Fig. 5.5C). The resulting force-indentation curves were analyzed using an elastic model for a 2D material in the form of a circular disk clamped along its circumference.[36] According to this model, the dependency of the applied force F on the vertical tip position δ can be written as linear addition of pretension σ^{2D} and the elastic modulus in 2D material E^{2D}:

$$F = \sigma^{2D}(\pi R)\left(\frac{\delta}{R}\right) + E^{2D}(q^3 R)\left(\frac{\delta}{R}\right)^3 \qquad \text{(Eq. 1)}$$

Here, R is the radius of the clamped thin film and $q = (1.05 - 0.15\nu - 0.16\nu^2)^{-1}$ is a dimensionless constant depending on the Poisson's ratio of the material. Considering the forces holding the film together are dominantly of a Van der Waals character, a Poisson's ratio ν = 0.33 was assumed, as previously used for freestanding nanoparticle membranes,[39,40] and protein monolayers grown on water,[41] which are all held together solely by Van der Waals interactions. The 2D approximation is only valid for systems where the film thickness h is considerably smaller than its diameter R, *i.e.* $R/h > 1$. In this case R = 1 μm and h = 2.5 nm, and thus the approximation holds for this system.

After the first contact with the decacyclene film, the tip induces elastic deformation fitting to the theory (Fig 5.5C, red curve). The fit is valid up to the point of non-elastic changes in the material, which appear as a change in the slope or a small drop in the force (Fig. 5.5C, red arrow; Fig. S5.8). These non-elastic changes were previously observed for graphene flakes as well as a consequence of cracks induced in the membrane.[42] Such points are hence not considered as full rupture of the decacyclene film, which is here defined as an event when the applied force decreases considerably (> 2 nN; Fig. 5C, green arrow). The distribution of penetration forces and the force inducing non-elastic deformations are shown in Figures 5.5D and 5.5E (see also Fig. S5.9A and B). On average, the thin film fails at an applied force of 26 ± 9 nN (N = 26) with cracks being induced at a force of 8 ± 4 nN (N = 27). Note that sharper AFM tips require smaller forces to induce failure of a material.[36,43] To objectively assess the material's properties, intrinsic parameters were needed.

The model described by Eq. 1 is a linear addition of the pretension and 2D elastic modulus. The fit approaches the prestress-independent limit when indented deep enough to produce nonlinear behavior. This condition is met here as, at deeper indentation, a successful fit is obtained that yields a 2D elastic modulus E^{2D}. An effective Young's modulus E can therefore be derived for the decacyclene film, by dividing the 2D elastic modulus with the film thickness as $E = E^{2D}/h$. An histogram of the effective Young's moduli thus derived shows a narrow distribution with the mean value at 6 ± 4 GPa (N = 27) (Fig. 5.5F, Fig. S5.9D). The resulting Young's modulus depends on the chosen Poisson's ratio of the material, which was chosen based on literary precedent (ν = 0.33). The data was also fitted with a Poisson's ratio for a graphene monolayer ν = 0.165, in which case the Young's modulus values increase by ~14%, indicating only a moderate influence of Poisson's ratio on the results. The elastic strength of the present decacyclene film is thus comparable with 2D MOFs (~5 GPa)[44], one order of magnitude less than 2D COFs (~26 GPa),[45] and three orders of magnitude less than pristine graphene (~1 TPa).[36]

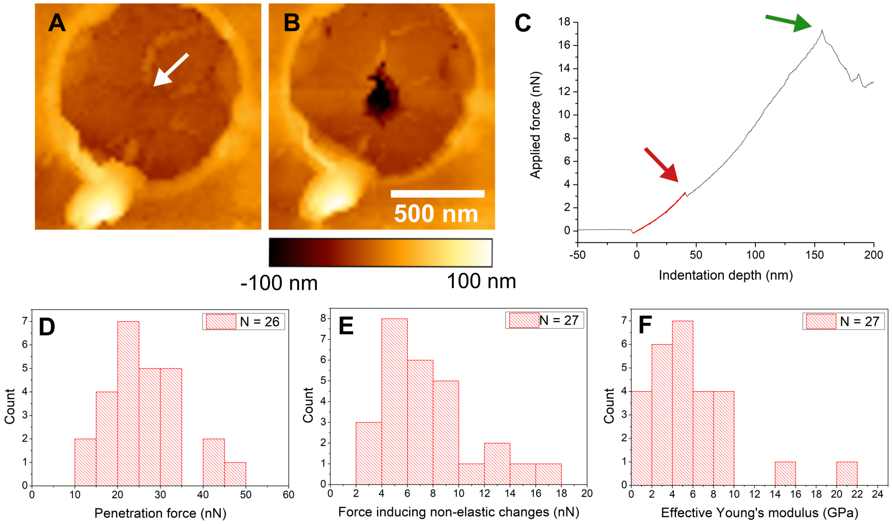

Figure 5.5 AFM nanoindentation of decacyclene films spanning over a 1 μm circular aperture. Representative AFM images before (A) and after (B) nanoindentation. White arrow in panel (A) indicates the point of the indentation with the AFM tip. (C) Representative force-indentation curve. Red curve shows the fit in the elastic regime. Red arrow points to a small drop in the slope of the curve. Above this point the fit of the elastic properties is no longer valid. The green arrow shows the breaking event when the thin film fully ruptures. (D) Histogram of the penetration force needed to rupture the thin film. (E) Histogram of the force inducing non-elastic changes in the thin films. (F) Effective Young's modulus of decacyclene film.

To conclude, it was shown that the small propellerene decacyclene is able to form stable, free-standing thin films, held together solely by collective van der Waals forces, and without the requirement of crosslinking or annealing. Computational modeling of the experimental conditions revealed the molecular reorientations and stacking interactions that take place at the air-water interface during Langmuir-Blodgett compression. Despite being held together by van der Waals forces, thin films were found stable enough to be free-standing over micrometer distances, which allowed quantification of their mechanical strength using AFM nanoindentation experiments. Thin films are found capable of withstanding point loads of 26 ± 9 nN, with a corresponding Young's modules of 6 ± 4 GPa, which is on par with reported 2D membranes. Although the present thin films are not yet capable for use in a device setting, these results constitute the starting point for further development of PAH-based, non-covalent thin films.

References

(1) Cohen-Tanugi, D.; Grossman, J. C. Nanoporous graphene as a reverse osmosis membrane: recent insights from theory and simulation. *Desalination* **2015,** *366*, 59.

(2) Wang, Z.; Wu, A.; Colombi Ciacchi, L.; Wei, G. Recent advances in nanoporous membranes for water purification. *Nanomaterials* **2018,** *8* (2), 65.

(3) Kim, W.-g.; Nair, S. Membranes from nanoporous 1D and 2D materials: A review of opportunities, developments, and challenges. *Chem. Eng. Sci.* **2013,** *104*, 908.

(4) Wang, L.; Boutilier, M. S. H.; Kidambi, P. R.; Jang, D.; Hadjiconstantinou, N. G.; Karnik, R. Fundamental transport mechanisms, fabrication and potential applications of nanoporous atomically thin membranes. *Nat. Nanotech.* **2017,** *12* (6), 509.

(5) Adiga, S. P.; Jin, C.; Curtiss, L. A.; Monteiro-Riviere, N. A.; Narayan, R. J. Nanoporous membranes for medical and biological applications. *WIRES Nanomed. Nanobiotech.* **2009,** *1* (5), 568.

(6) Song, N.; Gao, X.; Ma, Z.; Wang, X.; Wei, Y.; Gao, C. A review of graphene-based separation membrane: Materials, characteristics, preparation and applications. *Desalination* **2018,** *437*, 59.

(7) Makra, I.; Gyurcsányi, R. E. Electrochemical sensing with nanopores: A mini review. *Electrochem. Comm.* **2014,** *43*, 55.

(8) Park, H. B.; Kamcev, J.; Robeson, L. M.; Elimelech, M.; Freeman, B. D. Maximizing the right stuff: The trade-off between membrane permeability and selectivity. *Science* **2017,** *356* (6343).

(9) Nunes, S. P.; Culfaz-Emecen, P. Z.; Ramon, G. Z.; Visser, T.; Koops, G. H.; Jin, W.; Ulbricht, M. Thinking the future of membranes: Perspectives for advanced and new membrane materials and manufacturing processes. *J. Membrane Sci.* **2020,** *598*, 117761.

(10) Wei, G.; Quan, X.; Li, C.; Chen, S.; Yu, H. Direct growth of ultra-permeable molecularly thin porous graphene membranes for water treatment. *Environmental Science: Nano* **2018,** *5* (12), 3004.

(11) Cheng, W.; Campolongo, M. J.; Tan, S. J.; Luo, D. Freestanding ultrathin nano-membranes via self-assembly. *Nano Today* **2009,** *4* (6), 482.

(12) Biswas, A.; Bayer, I. S.; Biris, A. S.; Wang, T.; Dervishi, E.; Faupel, F. Advances in top-down and bottom-up surface nanofabrication: Techniques, applications & future prospects. *Adv. Colloid Interfac.* **2012,** *170* (1-2), 2.

(13) Thiruvengadathan, R.; Korampally, V.; Ghosh, A.; Chanda, N.; Gangopadhyay, K.; Gangopadhyay, S. Nanomaterial processing using self-assembly-bottom-up chemical and biological approaches. *Rep. Prog. Phys.* **2013,** *76* (6), 066501.

(14) Liu, X.; He, M.; Calvani, D.; Qi, H.; Gupta, K. B. S. S.; de Groot, H. J. M.; Sevink, G. J. A.; Buda, F.; Kaiser, U.; Schneider, G. F. Power generation by reverse electrodialysis in a single-layer nanoporous membrane made from core–rim polycyclic aromatic hydrocarbons. *Nat. Nanotech.* **2020,** *15* (4), 307.

(15) Wu, R.; Yue, W.; Li, Y.; Huang, A. Ultra-thin and high hydrogen permeable carbon molecular sieve membrane prepared by using polydopamine as carbon precursor. *Materials Letters* **2021,** *295*, 129863.

(16) Feng, X.; Schlüter, A. D. Towards macroscopic crystalline 2D polymers. *Angew. Chem. Int. Ed.* **2018,** *57* (42), 13748.

(17) Angelova, P.; Vieker, H.; Weber, N.-E.; Matei, D.; Reimer, O.; Meier, I.; Kurasch, S.; Biskupek, J.; Lorbach, D.; Wunderlich, K. A universal scheme to convert aromatic molecular monolayers into functional carbon nanomembranes. *ACS nano* **2013,** *7* (8), 6489.

(18) Pfeffermann, M.; Dong, R.; Graf, R.; Zajaczkowski, W.; Gorelik, T.; Pisula, W.; Narita, A.; Müllen, K.; Feng, X. Free-standing monolayer two-dimensional supramolecular organic framework with good internal order. *J. Am. Chem. Soc.* **2015,** *137* (45), 14525.

(19) Hisaki, I. Hydrogen-bonded porous frameworks constructed by rigid π-conjugated molecules with carboxy groups. *J. Incl. Phenom. Macro.* **2020,** *96* (3), 215.

(20) Lin, R.-B.; He, Y.; Li, P.; Wang, H.; Zhou, W.; Chen, B. Multifunctional porous hydrogen-bonded organic framework materials. *Chem. Soc. Rev.* **2019,** *48* (5), 1362.

(21) Suzuki, Y.; Tohnai, N.; Saeki, A.; Hisaki, I. Hydrogen-bonded organic frameworks of twisted polycyclic aromatic hydrocarbon. *Chem. Comm.* **2020,** *56* (87), 13369.

(22) Deng, J.-H.; Luo, J.; Mao, Y.-L.; Lai, S.; Gong, Y.-N.; Zhong, D.-C.; Lu, T.-B. π-π stacking interactions: Non-negligible forces for stabilizing porous supramolecular frameworks. *Science advances* **2020,** *6* (2), eaax9976.

(23) Das, S.; Chowdhury, A.; Pal, A. J. Alternating-current and direct-current responses of light-emitting devices based on decacyclene langmuir-blodgett films. *Phys. Status Solidi A* **2001,** *185* (2), 383.

(24) Acharya, S.; Parichha, T. K.; Talapatra, G. B. Spectroscopic properties of decacyclene assembled in Langmuir Blodgett film mixed with stearic acid. *Mol. Cryst. Liq. Cryst. Sci. Technol. Sect. C-Mol. Mat.* **2000,** *12* (1), 91.

(25) Amick, A. W.; Scott, L. T. Trisannulated benzene derivatives by acid catalyzed aldol cyclotrimerizations of cyclic ketones. Methodology development and mechanistic insight. *J. Org. Chem.* **2007,** *72* (9), 3412.

(26) Nishikata, Y.; Konishi, T.; Morikawa, A.; Kakimoto, M.-a.; Imai, Y. Preparation and monolayer thickness of Langmuir–Blodgett films of polyimides having various chemical structures. *Polym. J.* **1988,** *20* (3), 269.

(27) Vollhardt, D.; Fainerman, V. B. Progress in characterization of Langmuir monolayers by consideration of compressibility. *Adv. Colloid Interfac.* **2006,** *127* (2), 83.

(28) Ho, D. M.; Pascal Jr, R. A. Decacyclene: a molecular propeller with helical crystals. *Chem. Mater.* **1993,** *5* (9), 1358.

(29) The binding energy of the dimer was found to be 23.1 kcal mol^{-1} in terms of Gibbs free energy at PBE-D3(BJ)/6-31G(d,p)l.

(30) Wang, H.; Xu, X.; Li, L.; Yang, C.; Ji, H.-F. Optoelectronic property and sensing applications of crystalline nano/microwires of decacyclene. *Micro Nano Lett.* **2011,** *6* (9), 763.

(31) Schunack, M.; Lægsgaard, E.; Stensgaard, I.; Besenbacher, F. Bonding and ordering of decacyclene molecules on Cu (110) studied by scanning tunneling microscopy. *J. Chem. Phys.* **2002,** *117* (18), 8493.

(32) Schunack, M.; Linderoth, T. R.; Rosei, F.; Lægsgaard, E.; Stensgaard, I.; Besenbacher, F. Long jumps in the surface diffusion of large molecules. *Phys. Rev. Lett.* **2002,** *88* (15), 156102.

(33) Yao, Z.-F.; Wang, J.-Y.; Pei, J. Control of π–π stacking via crystal engineering in organic conjugated small molecule crystals. *Cryst. Growth Des.* **2018,** *18* (1), 7.

(34) Ermantraut, E.; Wohlfart, K.; Tichelaar, W. Perforated support foils with pre-defined hole size, shape and arrangement. *Ultramicroscopy* **1998,** *74* (1-2), 75.

(35) Roos, W. H.; Bruinsma, R.; Wuite, G. J. L. Physical virology. *Nature physics* **2010,** *6* (10), 733.

(36) Lee, C.; Wei, X.; Kysar, J. W.; Hone, J. Measurement of the elastic properties and intrinsic strength of monolayer graphene. *science* **2008,** *321* (5887), 385.

(37) Russo, C. J.; Passmore, L. A. Ultrastable gold substrates for electron cryomicroscopy. *Science* **2014,** *346* (6215), 1377.

(38) Bunch, J. S.; Verbridge, S. S.; Alden, J. S.; van der Zande, A. M.; Parpia, J. M.; Craighead, H. G.; McEuen, P. L. Impermeable atomic membranes from graphene sheets. *Nano Lett.* **2008,** *8* (8), 2458.

(39) He, J.; Kanjanaboos, P.; Frazer, N. L.; Weis, A.; Lin, X. M.; Jaeger, H. M. Fabrication and mechanical properties of large-scale freestanding nanoparticle membranes. *Small* **2010,** *6* (13), 1449.

(40) Kanjanaboos, P.; Joshi-Imre, A.; Lin, X.-M.; Jaeger, H. M. Strain patterning and direct measurement of Poisson’s ratio in nanoparticle monolayer sheets. *Nano Lett.* **2011,** *11* (6), 2567.

(41) Singh, A.; Konovalov, O. Measuring elastic properties of a protein monolayer at water surface by lateral compression. *Soft Matter* **2013,** *9* (10), 2845.

(42) Lee, G.-H.; Cooper, R. C.; An, S. J.; Lee, S.; van der Zande, A.; Petrone, N.; Hammerberg, A. G.; Lee, C.; Crawford, B.; Oliver, W. High-strength chemical-vapor-deposited graphene and grain boundaries. *Science* **2013,** *340* (6136), 1073.

(43) Denning, D.; Bennett, S.; Mullen, T.; Moyer, C.; Vorselen, D.; Wuite, G. J. L.; Nemerow, G.; Roos, W. H. Maturation of adenovirus primes the protein nano-shell for successful endosomal escape. *Nanoscale* **2019,** *11* (9), 4015.

(44) Hermosa, C.; Horrocks, B. R.; Martínez, J. I.; Liscio, F.; Gómez-Herrero, J.; Zamora, F. Mechanical and optical properties of ultralarge flakes of a metal–organic framework with molecular thickness. *Chem. Sci.* **2015,** *6* (4), 2553.

(45) Hao, Q.; Zhao, C.; Sun, B.; Lu, C.; Liu, J.; Liu, M.; Wan, L.-J.; Wang, D. Confined synthesis of two-dimensional covalent organic framework thin films within superspreading water layer. *J. Am. Chem. Soc.* **2018,** *140* (38), 12152.

(46) Pantelic, R. S.; Suk, J. W.; Magnuson, C. W.; Meyer, J. C.; Wachsmuth, P.; Kaiser, U.; Ruoff, R. S.; Stahlberg, H. Graphene: Substrate preparation and introduction. *J. Struct. Biol.* **2011,** *174* (1), 234.

(47) Frisch, M. J.; Trucks, G. W.; Schlegel, H. B.; Scuseria, G. E.; Robb, M. A.; Cheeseman, J. R.; Scalmani, G.; Barone, V.; Mennucci, B.; Petersson, G. A. Gaussian 09 Revision D. 01, 2009. *Gaussian Inc. Wallingford CT* **2009**.

(48) Grimme, S.; Antony, J.; Ehrlich, S.; Krieg, H. A consistent and accurate ab initio parametrization of density functional dispersion correction (DFT-D) for the 94 elements H-Pu. *J. Chem. Phys.* **2010,** *132* (15), 154104.

(49) Grimme, S.; Ehrlich, S.; Goerigk, L. Effect of the damping function in dispersion corrected density functional theory. *J. Comp. Chem.* **2011,** *32* (7), 1456.

(50) Ribeiro, R. F.; Marenich, A. V.; Cramer, C. J.; Truhlar, D. G. Use of solution-phase vibrational frequencies in continuum models for the free energy of solvation. *J. Phys. Chem. B* **2011,** *115* (49), 14556.

(51) Funes-Ardoiz, I.; Paton, R. S. **2016**. GoodVibes: GoodVibes v1.0.2. http://doi.org/10.5281/zenodo.595246.

(52) Legault, C. Y. *CYLview, 1.0 b, Université de Sherbrooke, **2009***, 2013.

(53) Berendsen, H. J. C.; van der Spoel, D.; van Drunen, R. GROMACS: a message-passing parallel molecular dynamics implementation. *Comput. Phys. Commun.* **1995,** *91* (1-3), 43.

(54) Lindahl, E.; Hess, B.; Van Der Spoel, D. GROMACS 3.0: a package for molecular simulation and trajectory analysis. *Mol. Mod. Ann.* **2001,** *7* (8), 306.

(55) Van Der Spoel, D.; Lindahl, E.; Hess, B.; Groenhof, G.; Mark, A. E.; Berendsen, H. J. C. GROMACS: fast, flexible, and free. *J. Comp. Chem.* **2005,** *26* (16), 1701.

(56) Hess, B.; Kutzner, C.; Van Der Spoel, D.; Lindahl, E. GROMACS 4: algorithms for highly efficient, load-balanced, and scalable molecular simulation. *J. Chem. Theo. Comp.* **2008,** *4* (3), 435.

(57) Pronk, S.; Páll, S.; Schulz, R.; Larsson, P.; Bjelkmar, P.; Apostolov, R.; Shirts, M. R.; Smith, J. C.; Kasson, P. M.; van der Spoel, D. GROMACS 4.5: a high-throughput and highly parallel open source molecular simulation toolkit. *Bioinformatics* **2013,** *29* (7), 845.

(58) Abraham, M. J.; Murtola, T.; Schulz, R.; Páll, S.; Smith, J. C.; Hess, B.; Lindahl, E. GROMACS: High performance molecular simulations through multi-level parallelism from laptops to supercomputers. *SoftwareX* **2015,** *1*, 19.

(59) Páll, S.; Abraham, M. J.; Kutzner, C.; Hess, B.; Lindahl, E.; **2014**, Tackling exascale software challenges in molecular dynamics simulations with GROMACS.

(60) York, D. M.; Darden, T. A.; Pedersen, L. G. The effect of long-range electrostatic interactions in simulations of macromolecular crystals: A comparison of the Ewald and truncated list methods. *J. Chem. Phys.* **1993,** *99* (10), 8345.

(61) Bussi, G.; Donadio, D.; Parrinello, M. Canonical sampling through velocity rescaling. *J. Chem. Phys.* **2007,** *126* (1), 014101.

(62) Horn, H. W.; Swope, W. C.; Pitera, J. W.; Madura, J. D.; Dick, T. J.; Hura, G. L.; Head-Gordon, T. Development of an improved four-site water model for biomolecular simulations: TIP4P-Ew. *J. Chem. Phys.* **2004,** *120* (20), 9665.

(63) Harris, J. G. Liquid-vapor interfaces of alkane oligomers: structure and thermodynamics from molecular dynamics simulations of chemically realistic models. *J. Phys. Chem.* **1992,** *96* (12), 5077.

(64) Vega, C.; De Miguel, E. Surface tension of the most popular models of water by using the test-area simulation method. *J. Chem. Phys.* **2007,** *126* (15), 154707.

(65) Chen, F.; Smith, P. E. Simulated surface tensions of common water models. *J. Chem. Phys.* **2007,** *126*, 221101.

(66) Jorgensen, W. L.; Maxwell, D. S.; Tirado-Rives, J. Development and testing of the OPLS all-atom force field on conformational energetics and properties of organic liquids. *J. Am. Chem. Soc.* **1996,** *118* (45), 11225.

(67) Kaminski, G. A.; Friesner, R. A.; Tirado-Rives, J.; Jorgensen, W. L. Evaluation and reparametrization of the OPLS-AA force field for proteins via comparison with accurate quantum chemical calculations on peptides. *J. Phys. Chem. B* **2001,** *105* (28), 6474.

(68) Martin, M. G. Comparison of the AMBER, CHARMM, COMPASS, GROMOS, OPLS, TraPPE and UFF force fields for prediction of vapor–liquid coexistence curves and liquid densities. *Fluid Phase Equilibr.* **2006,** *248* (1), 50.

(69) Dodda, L. S.; Cabeza de Vaca, I.; Tirado-Rives, J.; Jorgensen, W. L. LigParGen web server: an automatic OPLS-AA parameter generator for organic ligands. *Nucleic Acid Res.* **2017,** *45* (W1), W331.

(70) Marenich, A. V.; Jerome, S. V.; Cramer, C. J.; Truhlar, D. G. Charge model 5: An extension of Hirshfeld population analysis for the accurate description of molecular interactions in gaseous and condensed phases. *J. Chem. Theo. Comp.* **2012,** *8* (2), 527.

(71) Frisch, M. J.; Trucks, G. W.; Schlegel, H. B.; Scuseria, G. E.; Robb, M. A.; Cheeseman, J. R.; Scalmani, G.; Barone, V.; Petersson, G. A.; Nakatsuji, H.; Gaussian, Inc., Wallingford CT, 2016.

(72) Martínez, J. M.; Martínez, L. Packing optimization for automated generation of complex system's initial configurations for molecular dynamics and docking. *J. Comp. Chem.* **2003,** *24* (7), 819.

(73) Martínez, L.; Andrade, R.; Birgin, E. G.; Martínez, J. M. PACKMOL: a package for building initial configurations for molecular dynamics simulations. *J. Comp. Chem.* **2009,** *30* (13), 2157.

(74) Van der Spoel, D.; Lindahl, E.; Hess, B.; Van Buuren, A. R.; Apol, E.; Meulenhoff, P. J.; Tieleman, D. P.; Sijbers, A.; Feenstra, K. A.; Van Drunen, R. *Gromacs User Manual version 4.5.6*, **2010**.

(75) Fine, R. A.; Millero, F. J. Compressibility of water as a function of temperature and pressure. *J. Chem. Phys.* **1973,** *59* (10), 5529.

(76) Humphrey, W.; Dalke, A.; Schulten, K. VMD: visual molecular dynamics. *J. Mol. Graphics* **1996,** *14* (1), 33.

(77) Roos, W. H. In *Single Molecule Analysis*; Springer, **2011**.

(78) Ribeiro, A. A. S. T.; Horta, B. A. C.; Alencastro, R. B. D. MKTOP: a program for automatic construction of molecular topologies. *J. Brazil. Chem. Soc.* **2008,** *19* (7), 1433.

(79) Jorgensen, W. L.; Severance, D. L. Aromatic-aromatic interactions: free energy profiles for the benzene dimer in water, chloroform, and liquid benzene. *J. Am. Chem. Soc.* **1990,** *112* (12), 4768.

(80) Gowers, R. J.; Linke, M.; Barnoud, J.; Reddy, T. J. E.; Melo, M. N.; Seyler, S. L.; Domanski, J.; Dotson, D. L.; Buchoux, S.; Kenney, I. M. *MDAnalysis: a Python package for the rapid analysis of molecular dynamics simulations*; Los Alamos National Lab.(LANL), Los Alamos, NM (United States), 2019.

Experimental

Sample preparation. Decacyclene was synthesized according to the procedure of Amick and Scott.[25] Identity and purity of the material were checked using ^{1}H NMR spectroscopy on a Bruker AV500 NMR instrument equipped with a BBFO probe head for 5 mm outer diameter tubes. Spectra were recorded at 500 MHz for ^{1}H using deuterated chloroform obtained from a commercial source (EurIsoTop®). Thin film samples were prepared on a Langmuir–Blodgett trough (KSV NIMA, Finland) filled with Millipore® Ultrapure water (18 MΩ cm^{-1}). The surface pressure was measured with a Wilhelmy balance. A solution of decacyclene in chloroform (75 µl, 1.1 mM) was carefully spread on the water surface using a micropipette. After 30 min, the surface was compressed by two barriers with a fixed speed of 2 mm min^{-1} to reach a certain surface. Thin film samples were transferred onto silicon wafers at constant pressure by the Langmuir–Schäfer method. Samples were transferred onto copper or gold TEM grids following standard procedures.[46] Copper substrate for IR experiments was obtained from Puratonic® and had a thickness of 0.025 mm and a 99.999% purity.

Thin film characterization. AFM images of the thin films on Si/SiO_2 wafers were recorded on a JPK Nano Wizard Ultra Speed machine with a silicon 254 probe (AC 160 TS, Asylum Research) with 300 kHz nominal resonance frequency. The images were scanned in intermittent contact mode in air at room temperature. The SEM images were recorded by using an FEI NOVA nano SEM 200 scanning electron microscope.

Density Functional Theory. Equilibrium geometries were computed at the PBE/6-31G(d,p) level of theory using the Gaussian 09 Rev. D.01 program suite,[47] using the D3(BJ) dispersion correction.[48,49] The geometry convergence criteria were set to tight (Opt = tight; Max. Force = $1.5\cdot10^{-7}$, Max. Displacement = $6.0\cdot10^{-7}$), and an internally defined super-fine grid size was used (SCF=tight, Int=VeryFineGrid), which is a pruned 175,974 grid for first-row atoms and a 250,974 grid for all other atoms. Free Gibbs energies were computed using Equation S1, in which ΔE_{gas} is the gas-phase energy (electronic energy) and $\Delta G^{T}_{\mathrm{gas,QH}}$ (T = 293.15 K, p = 1 atm., C = 1 M) is the sum of corrections from the electronic energy to the free Gibbs energy in the quasi-harmonic oscillator approximation, including zero-point-vibrational energy. The $\Delta G^{T}_{\mathrm{gas,QH}}$ were computed using the quasi-harmonic approximation in the gas phase according to the work of Truhlar in which vibrational frequencies lower than 100 cm^{-1} were raised to 100 cm^{-1} to correct for the breakdown of the harmonic oscillator model for the free energies of low-frequency vibrational modes.[50,51] Stationary points were checked to have no imaginary frequencies for local minima, and one imaginary frequency for the transition state structure. All DFT structures were illustrated using CYLview.[52]

$$\Delta G^{T}_{\mathrm{gas}} = \Delta E_{\mathrm{gas}} + \Delta G^{T}_{\mathrm{gas,QH}} \qquad \text{(Eq. S1)}$$

*Molecular Dynamics***.** All MD simulations were carried out using the GROMACS 2016 software suite.[53-59] The Particle Mesh Ewald (PME) method was employed to accurately account for electrostatic interactions.[60] The cut-off for Coulomb and Lennard-Jones interactions was set to 10 Å. During the NVT simulation the temperature was kept fixed with the V-rescale coupling method.[61]

Simulation setup. The model for a body of water, comprised of 4139 water molecules, was simulated in a periodic box (5.0 x 5.0 x 20.0 nm^3) using the TIP4P-Ew/2004 force field.[62] The water surface tension was used as defined within the GROMACS software suite (Equation S2):

$$\gamma_{water} = \frac{1}{2} L_z [P_{zz} - \frac{1}{2}(P_{xx} + P_{yy})] \qquad \text{(Eq. S2)}$$

where L_z is the box length in the z direction, P_{xx}, P_{yy} and P_{zz} are the respective xx, yy and zz element of the pressure tensor,[63] and the ½ originates from the presence of two x-y plane surfaces in the system. The system was first energetically minimized and then equilibrated for 8 ns with NVT at 300 K to obtain an average surface tension of γ_{water} = 58.46 mN m^{-1}. This value is in good agreement with previous studies.[64,65] The water model was further validated using a radial distribution function and density analysis (Fig. S5.4).

Simulation setting for the water-propellerene interfaces. Decacyclene molecules were simulated using the OPLS-AA force field (see Table S1)[66-68] and LigParGen[69] parameterization with charges calculated with the CM5 model[70] using the Gaussian 16 Rev. C.01 program suite.[71] Input geometries for decacyclene were obtained from DFT (*vide supra*).

Simulation run. Random input positions of 30 or 60 decacyclene molecules on both water surfaces were generated using the PACKMOL18 program.[72,73] Having two independent water-decacyclene interfaces provides a more symmetric MD simulation box and increases the statistics of the results by averaging on both interfaces. Moreover, the presence of the decacyclene molecule on both sides avoids the diffusion of water molecules through the periodic boundary condition along the z-axis. The two interfaces can be considered independent due to the thickness (5 nm) of the water box and the vacuum space (at least 5 nm on each side) above each interface along the z-axis. For each simulation, the system was first equilibrated with NVT at 70 K for 5 ns, and the temperature then raised to 300 K for another 5 ns. After these pre-equilibration simulations, the production run consists in NVT simulations were ran at 300 K for 10 ns. The final configuration extracted from the production run was used as a starting point for the subsequent NPT surface tension simulations. These series of simulations are repeated independently three times starting from a different random packing, in order to check the effect of initial conditions on the final results.

Series of simulations were repeated independently three times, starting from different random packings, in order to counteract the effect of initial conditions on the final results.

Surface Tension calculations

Surface tension coupling for surfaces parallel to the xy-plane was used, using normal pressure coupling for the z-direction, while the surface tension is coupled to the x/y dimensions of the box. The surface pressure was then increased stepwise, to generate pressure-area isotherms. At each chosen surface pressure (0, 3, 10, 20, 30, 40, 50 mN m^{-1}), the surface tension coupling molecular dynamics were performed while monitoring the change of the area in the x-y plane. In order to execute the constant surface tension simulations, the Berendsen pressure coupling was used.[74] For this coupling method to be effective, a value for the compressibility is required, which is close to the real compressibility of the system, namely 4.5×10^{-5} bar^{-1}. [75] Simulations were stopped after 10 ns, at which point an equilibrium state was reached. Data presented in the manuscript was obtained averaging the values on the last 10 ns of each corresponding simulation. The x-y area values are equilibrated enough with an error around ±0.05 Å. (Fig. S5.3). These series of simulations were repeated independently starting from each last equilibration simulation described in the previous paragraph, in order to increase the reproducibility of the results.

All MD results were illustrated using Visual Molecular Dynamics (VMD).[76]

AFM nanoindentation experiments

AFM imaging and nanoindentation of the TEM grid supported freestanding thin films was performed with an JPK Nano Wizard Ultra Speed AFM.[35,36] The TEM grid (with apertures of 1 µm in diameter) was immobilized by tape on top of a glass slide and imaged in QI^{TM} mode. The experiments were performed in air at room temperature (22°C) using SNL-10A cantilevers (Bruker) with a calibrated spring constant of 0.432 ± 0.003 Nm^{-1} and a silicon nitride tip with nominal radius of 2 nm. The imaging force was ~400–600 pN. After imaging the free-standing thin films, the intact thin films were indented in the center by a force up to 50 nN with an indentation velocity of 300 nm sec^{-1}. Force-distance curves were recorded during indentation. After indentation, the same spot was imaged again.

AFM image analysis

Both the AFM images and the force curves were processed using JPK Data Processing software. Representative images before and after indentation are shown at Fig. S5.6. The height profile of a thin film spanning over a circular aperture is plotted in Fig. S5.7. The profile exhibits a dip in height in the middle, as also previously reported for suspended graphene membranes,[36] and a small elevation of the thin film height around the circumference of the aperture.

AFM force-indentation curves analysis

In brief, the nanoindentation experiment yield the deflection of the cantilever as a function of the Z-piezo displacement. This dependency was converted to the applied force versus the vertical distance between the tip and the sample surface by subtracting the deflection of the cantilever itself.[77] The contact point between the tip and the thin film was defined as a point, when the force-indentation curve starts exhibiting non-zero force. The initial increase in the force-indentation response up to the first apparent change in the slope or a small drop in the force (< 2 nN) was fitted using Eq. 1 according to the model for elastic properties of a 2D material described in Ref [36]. Two parameters were derived from the fit: prestress in 2D and elastic modulus in 2D. By dividing the 2D elastic modulus by the film thickness h = 2.5 nm, the effective Young's modulus of the decacyclene film is obtained. The analysis was done independently on two sets of data, the curves with the small drop in the force increase (Fig. S5.8A; N = 7), and the curves with apparent change in the slope (Fig. S5.8B; N = 20). Figure S5.9 shows the histograms of the pre-tension in 2D, the effective Young's modulus, the force inducing non-elastic changes in the thin film (when a small drop or slope change occurs), and the force needed to fully rupture the thin film. The latter is being defined as a force drop > 2 nN. The histograms show comparable distributions for the two subsets of data and hence the data from both subsets were combined and included into overall statistical analysis of the mechanical properties of the decacyclene films.

Supplementary Figure and Tables

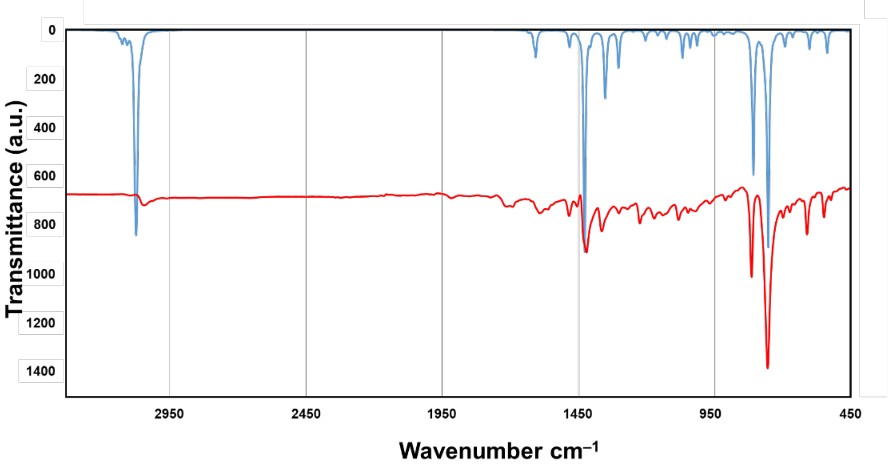

Figure S5.1 Infrared spectra of decacyclene as computed for the dimer at the PBE/6-31G(d,p) level (blue), and experimentally recorded for the powder (red).

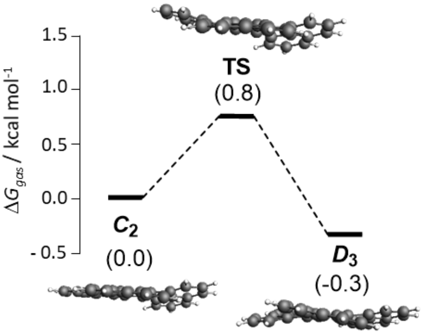

Figure S5.2 Potential energy surface for the interconversion of decacyclene between its C_2 and D_3 conformer. Energies are expressed as Gibbs free energies in kcal mol^{-1}, as computed at PBE-D3(BJ)/6-31G(d,p).

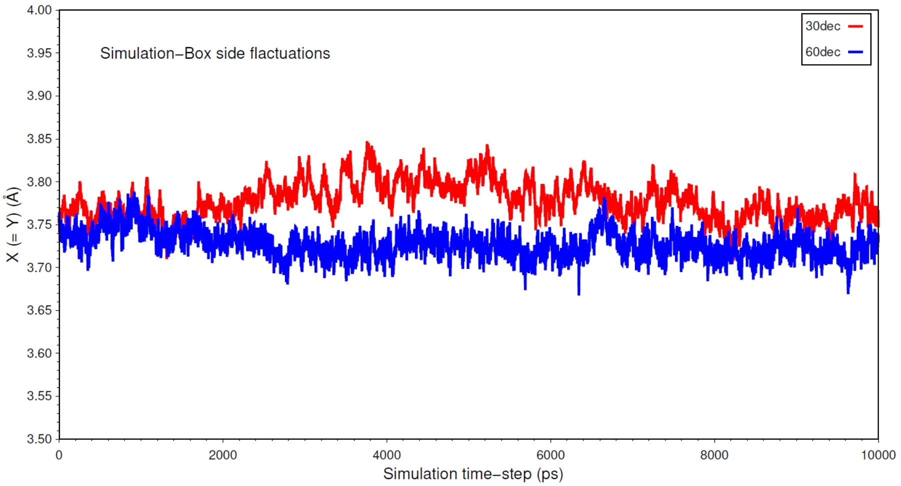

Figure S5.3 Fluctuations of the simulation box side X (= Y) during the Surface Tension MD at 30 mN m^{-1} for 30 and 60 decacyclene systems, respectively in red and blue color. The simulation time-steps are reported in ps.

Table S5.1 Assigned force field types for decacyclene molecule list for reproduce the simulation.[78]

OPLS-AA atom type	**Description**
opls_145	Benzene C - 12 site.[79] Use #145B for biphenyl
opls_146	Benzene H - 12 site.
opls_145B	Biphenyl C1

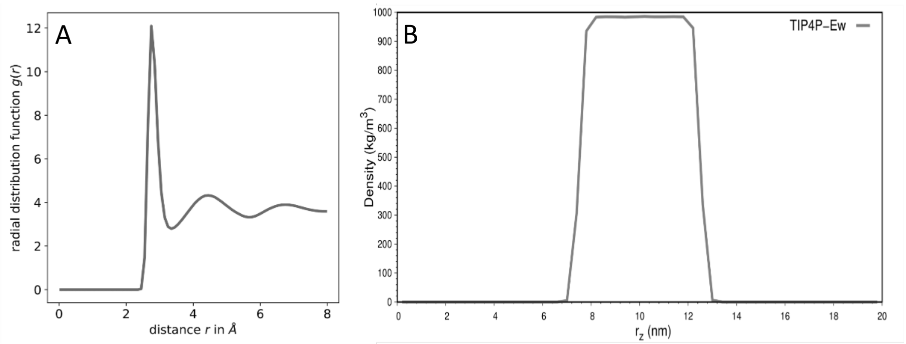

Figure S5.4 (A) O-O radial distribution function *g*(r) for water, calculated using the MDAnalysis tool.[80] (B) Density curve (kg m^{-3}) of the water molecules along the *z*-coordinate r_z (nm) of the water box.

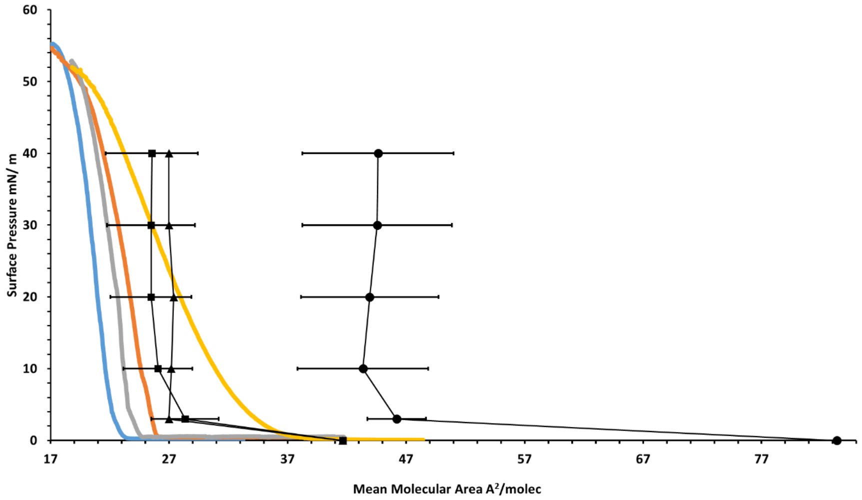

Figure S5.5 Representative experimental Langmuir-Blodgett isotherms for two consecutive compression/decompression cycles on a single sample, showing surface pressure as a function of mean molecular area. Black lines are isotherms computed using MD simulations for a system containing 60 (+) rotating decacyclene molecules (■), 60 (-) rotating molecules (●), and a system with a mixture of 30 (+) and 30 (-) rotating decacyclene molecules (▲).

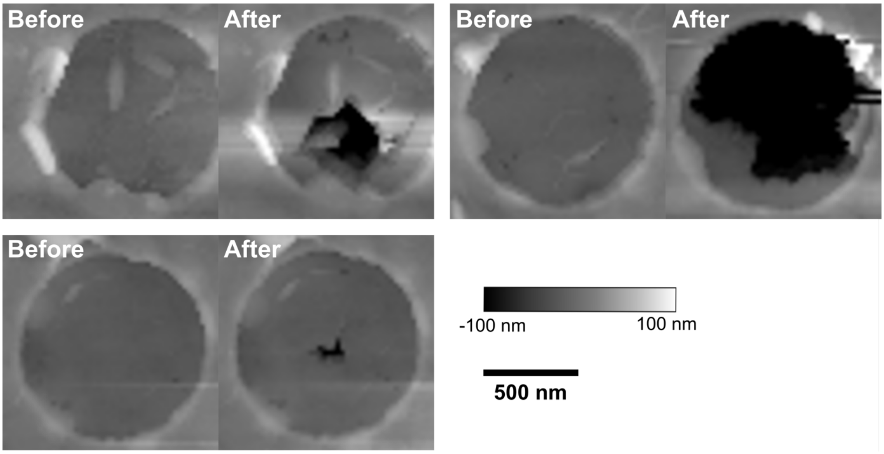

Figure S5.6 Representative AFM images of the decacyclene film spanning over the circular apertures before and after the nanoindentation with a force load of 50 nN.

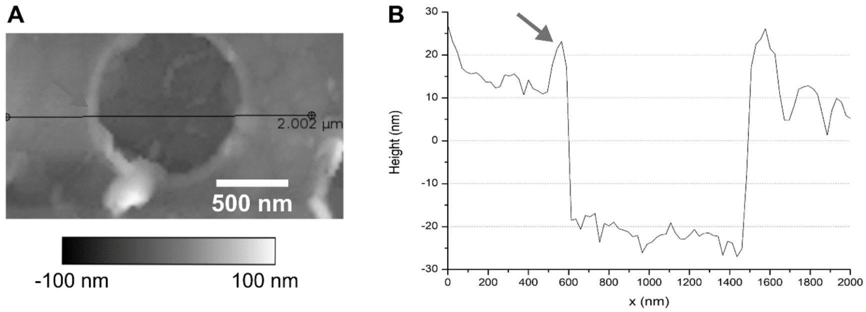

Figure S5.7 (A) AFM image of a thin film spanning over the circular aperture with a cross-section line highlighted. (B) Corresponding height profile along the cross-section line. Arrows in both panels point to the increase in height at the rim of the aperture, visible as a lighter color in the AFM image.

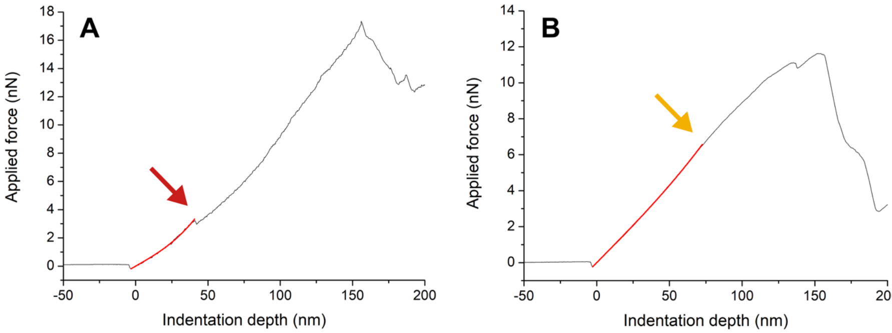

Figure S5.8 Representative force-indentation curves. Curves displaying (A) small drop in the applied force (arrow), and (B) change in the slope (arrow). Red lines represent fits of the experimental data according to Eq. 1.[36]

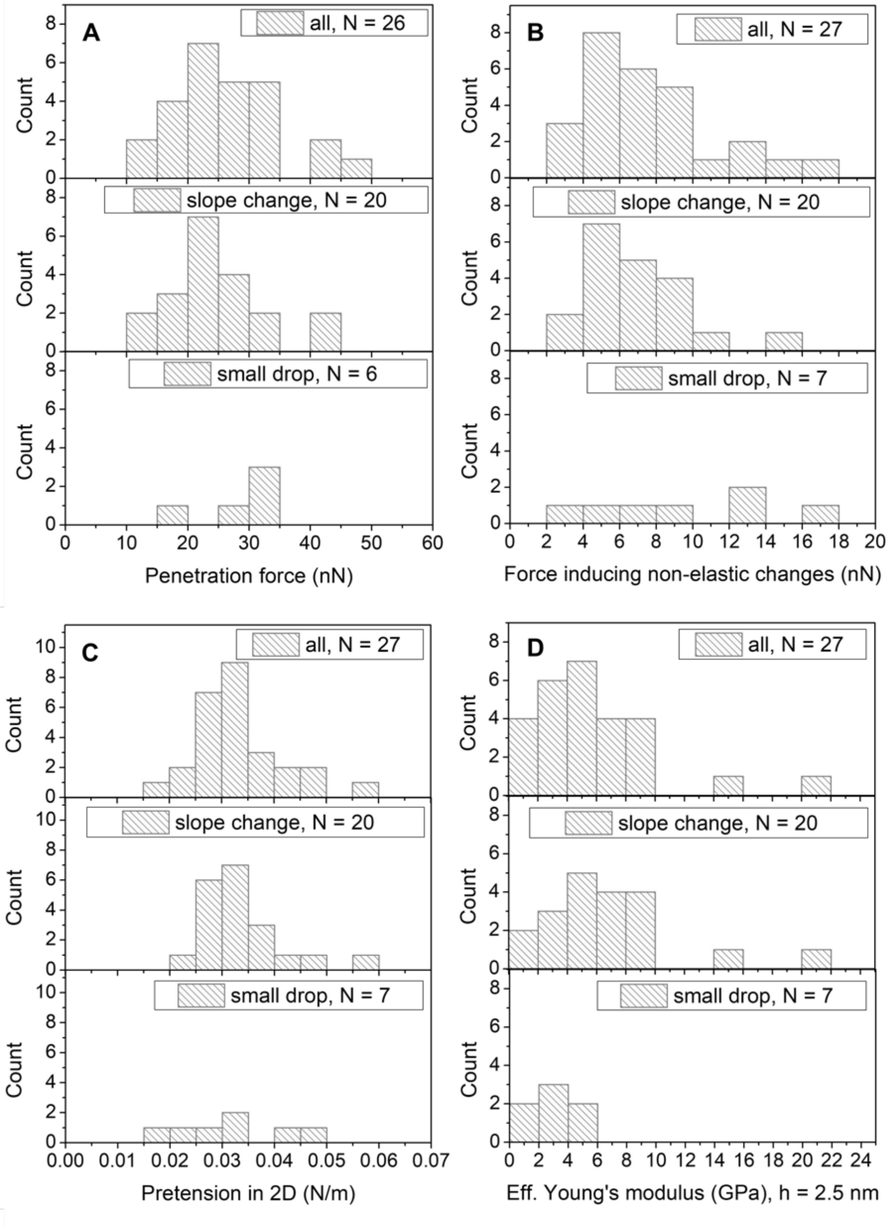

Figure S5.9 Mechanical parameters from the AFM nanoindentation experiments. Histograms of the parameters from all the acquired force-indentation curves, from the subset of the curves with an apparent change in the slope, and from the subset with the small drop in the force are shown. (A) Penetration force needed to fully rupture the thin film (demonstrated as a drop in the applied force > 2 nN). (B) Force inducing non-elastic changes. *i.e.* the force when the first small drop or the slope change occurs. (C) Pretension in 2D material as defined in Ref. [36]. (D) Effective Young's modulus of decacyclene film.